Age-related changes in the function and structure of the peripheral sensory pathway in mice

AGE-RELATED CHANGES IN THE FUNCTION AND STRUCTURE OF THE PERIPHERAL SENSORY PATHWAY IN MICE

Canta A[1*]., Chiorazzi A[1*]., Carozzi V[1]., Meregalli C[1]., Oggioni N[1].,Bossi M [1]., Rodriguez-Menendez V[1]., Avezza F [1]., Crippa L. [2], Lombardi R[3]., de Vito G.[4,5], Piazza V[4]., Cavaletti G[1]., Marmiroli P[1].

[1] Experimental Neurology Unit and Milan Center for Neuroscience, School of Medicine and Surgery, University of Milano-Bicocca, via Cadore 48, 20900 Monza, Italy

[2] Istovet, via Tobagi 15, 20842 Besana in Brianza, Italy

[3] IRCCS Foundation "Carlo Besta" Neurological Institute, 3rd Neurology Unit, Milano, Italy

[4] Center for Nanotechnology Innovation @NEST, Istituto Italiano di Tecnologia, piazza San Silvestro 12, 56127 Pisa, Italy

[5] NEST, Scuola Normale Superiore, piazza San Silvestro 12, 56127, Pisa, Italy

* Equally contributed to the study

Corresponding author:

Dr. Alessia Chiorazzi
Experimental Neurology Unit,
School of Medicine and Surgery
University of Milano-Bicocca, v. Cadore 48, 20900 Monza, Italy
Phone: +39 02 6448 8122
Fax: +39 02 6448 8250
Mail: alessia.chiorazzi@unimib.it

ABSTRACT

This study is aimed at describing the changes occurring in the entire peripheral nervous system (PNS) sensory pathway along a 2-year observation period in a cohort of C57BL/6 mice.

The neurophysiological studies evidenced significant differences in the selected time points corresponding to childhood, young adulthood, adulthood and aging (i.e. 1, 7, 15 and 25 month of age), with a parabolic course as function of time.

The pathological assessment allowed to demonstrate signs of age-related changes since the age of 7 months, with a remarkable increase in both peripheral nerves and dorsal root ganglia (DRG) at the subsequent time points. These changes were mainly in the myelin sheaths, as also confirmed by the Rotating-Polarization Coherent-Anti-stokes-Raman-scattering (RP-CARS) microscopy analysis. Evident changes were also present at the morphometric analysis performed on the peripheral nerves, DRG neurons and skin biopsies.

This extensive, multimodal characterization of the PNS changes in aging provides the background for future mechanistic studies allowing the selection of the most appropriate time points and readouts according to the investigation aims.

Key words: Aging, peripheral nervous system, morphometric analysis, nerve conduction velocity, mice, RP-CARS

1 INTRODUCTION

According to the United Nations (World Population Prospect, 2015 revision, available at http://esa.un.org/unpd/wpp/publications) worldwide life expectancy at birth is projected to rise from 70 years in 2010-2015 to 77 years in 2045-2050 and to 83 years in 2095-2100. This remarkable demographic trend, associated with more careful medical assessment, is accompanied by a parallel increase in the occurrence of diseases typically associated with aging. In the field of neurological disorders, attention has been focused mostly on central nervous system neurodegenerative diseases (e.g. Parkinson's and Alzheimer's disease) in view of their frequency and their major, clearly perceived impact on the daily life activities and autonomy of the affected persons. However, also age-related changes occurring in the sensory component of the peripheral nervous system (PNS) are frequent and may severely compromise the conditions of aged persons. The overall prevalence of peripheral neuropathies is around 2% in the general population, but it raises up to 15% in people over the age of 40 (Bharucha, et al., 1991,Savettieri, et al., 1993). *Ad hoc* epidemiologic studies suggested that the prevalenceof peripheral neuropathies steadily increases over the age of 65 (Beghi and Monticelli, 1998,Monticelli and Beghi, 1993), but patients were not stratified for the presence of concomitant diseases typically occurring with aging and which are potentially able to impair PNS functioning (e.g. diabetes, vitamin deficiency, renal insufficiency, toxics exposure) (Martyn and Hughes, 1997).

A few epidemiologic studies confirm that peripheral neuropathies not only steadily increase in frequency, but also have worse progression over 65 years of age (Beghi and Monticelli, 1998,Gregg, et al., 2004,Leblhuber, et al., 2011). However, their frequency in elderly persons is probably still underestimated and their importance in one of the most vulnerable and frail category of population is not yet properly admitted.

Clinical, neurophysiological and pathological changes affecting particularly the sensory component of the PNS functioning are well-established in elderly persons, with impaired vibration perception more evident in the distal parts of the limbs, reduced amplitude of nerve potentials and decreased density of nerve fibers in sural nerve as well as in skin biopsies (Gregg, et al., 2004,Mold, et al., 2004,Ward, et al., 2015). Impaired function of the sensory PNS considerably contributes to other morbidities (Richardson, 2002) and results in pain, foot deformities, amputations and skin ulcerations as well as in increased risk of falls (Leblhuber, et al., 2011,Ward, et al., 2014). Motor impairment strictly dependent on peripheral nerve alterations is, by contrast, less frequent and the evident age-related reduction in strength

and motor performances is generally due to a multi-factorial sum of events, including musculoskeletal changes (Manini and Clark, 2012). Moreover, sensory function decline has been recognized to be significantly associated with decline in strength in older adults even in the presence of normal motor nerve functioning (Ward, et al., 2015).

Although most acquired peripheral neuropathies occur in elderly people in the course of systemic diseases or are caused by toxics exposure or trauma, in the absence of known causes of peripheral neuropathy it can be assumed that progressive nerve degeneration is *per se* a feature of aging, independently from other concurrent medical conditions. To support this hypothesis, functional, morphologic, and biochemical changes have been described in the PNS of aged subjects as well as in animal models (Ceballos, et al., 1999,Deshpande, et al., 2008,Fujimaki, et al., 2009,Jeronimo, et al., 2008,Melcangi, et al., 2003,Shen, et al., 2011,Verdú, et al., 1996,Verdú, et al., 2000). Among the possible mechanisms responsible for age-related PNS changes, poor nerve circulation, reduced regeneration from subclinical damage, decreased physiologic turnover of peripheral nerve components and increased susceptibility to local nerve entrapment have been suggested (Ceballos, et al., 1999,Suzuki, 2013).

In order to investigate on PNS aging a few studies have been performed in rodents (Ceballos, et al., 1999,Jeronimo, et al., 2008,Melcangi, et al., 2003,Shen, et al., 2011,van Nes, et al., 2008,Verdú, et al., 1996,Verdú, et al., 2000). However, controversies still exist about the rate of nerve degeneration during the lifetime of the animals, and about possible differences existing among nerves and animal species (Schmelzer and Low, 1987). Moreover, despite the knowledge that pathological changes are not uniformly distributed in the PNS (Ceballos, et al., 1999) and that clinical impairment is more severe in the longer leg nerves than in the shorter ones innervating the arms (Leblhuber, et al., 2011), no studies evaluated in detail the entire sensory pathway, from the distalmost part represented by skin nerve fibers up to the dorsal root ganglia (DRG).

The aim of this study is to define, using morphological/morphometric and neurophysiological approaches, the pattern of nervous system changes occurring during aging in the entire peripheral sensory pathway from the skin endings to the DRG neurons, in the same cohort of C57BL/6 mice examined longitudinally at different time points over a period of 2 years. Moreover, sampling two different nerves, one more distal (caudal) and one more proximal (sciatic), length-dependent features of normal aging will be compared.

2 MATERIALS AND METHODS

2.1 Animal husbandry

Sixty-six female C57BL/6 mice (Harlan Italy, Corezzana, Italy) aged 4 weeks at the beginning of the study were used. The care and husbandry of animals were in conformity with the institutional guidelines in compliance with national (D. L.vo 26/2014, Gazzetta Ufficiale della Repubblica Italiana, n.61, March 14th 2014) and international laws and policies (European Union directive 2010/63/UE; Guide for the Care and Use of Laboratory Animals, U.S. National Research Council, 1996). The study plan was approved by the Ethics Committee of the University of Milan Bicocca (n. 0035125/12). Animals were housed in a limited access animal facility where room temperature and relative humidity were set at 20 ± 2 °C and 55 ± 10%, respectively. Artificial lighting provided a 12 h light/12 h dark (7 a.m.–7 p.m.) cycle. The general condition of the animals was assessed daily, body weight changes were evaluated monthly while caudal and digital nerve conduction studies were performed every 2 months in all animals for a period of 2 years from the study start. Every two months three randomly selected mice were sacrificed under isoflurane deep general anesthesia and the isolated sciatic nerve as well as ventral caudal nerve, L4-L5 DRG and skin samples were collected and processed for morphological and morphometric analysis.

2.2 Hematology and blood chemistry

At 17, 21 months of age and at the end of the period of observation (25 months of age), whole blood was obtained from all sacrificed animals through caval vein puncture and serum was obtained by the centrifugation of clotted blood at 2.500g for 15 min at 4°C and used for determination of the levels of urea, creatinine, aspartate aminotransferase (AST), and alanine aminotransferase (ALT) as markers of kidney and liver function with an automatic MIRA PLUS system (Horiba ABX Diagnostic, Montpellier, France) (Cavaletti, et al., 2013).

2.3 Neurophysiology

The neurophysiological evaluations were performed in a temperature-controlled room, under isoflurane anesthesia, monitoring animal vital signs and body temperature. The nerve conduction velocity (NCV) and the amplitude of the sensory potential (SAP) were measured in the caudal and digital nerves using an electromyography apparatus (Myto2 ABN Neuro, Firenze, Italy). Caudal nerve neurophysiological assessments were performed by placing a couple of recording needle electrodes at the base of the tail and a couple of stimulating needle electrodes 3.5 cm distally to the

recording points. Similarly, the digital nerve assessments were performed by placing the positive recording electrode in the thigh, the negative recording electrode close to the ankle bone and the positive and negative stimulating electrodes close to the fourth toe near the digital nerve and under the paw respectively. The intensity, duration and frequency of stimulation were set up in order to obtain optimal results, as previously described in detail (Carozzi, et al., 2010,Carozzi, et al., 2015,Meregalli, et al., 2015,Renn, et al., 2011).

2.4 Pathological evaluation of peripheral nerves and DRG

Every 2 months 3 animals were sacrificed under deep anesthesia. Sciatic and ventral caudal nerves were isolated at the same anatomical point (mid-thigh or 1 cm from the base of the tail, respectively) and dissected out without stretching. The specimens were fixed by immersion in 3% glutaraldehyde in 0.12 M phosphate buffer solution, post-fixed in OsO_4, epoxy resin embedded and used for light and electron microscopic observations and for morphometric analysis. L4-L5 DRG were carefully isolated and collected in 3 animals. The specimens were fixed by immersion in 4% paraformaldehyde and 2% glutaraldehyde in 0.12 M phosphate buffer solution, post-fixed in OsO_4, epoxy resin embedded and used for light and electron microscopic observations and for morphometric analysis. Semi-thin sections (1 μm) were prepared and stained with toluidine blue and examined with a Nikon Eclipse E200 light microscope (Leica Microsystems GmbH, Wetzlar, Germany). Ultrathin sections were obtained from unselected tissue blocks of peripheral nerves and DRG using a Reichert-Jung Ultracut E ultramicrotome (Leica, Vienna, Austria), counterstained with uranyl acetate and lead citrate, and examined with a Philips CM-10 (FEI, Hillsboro, OR) transmission electron microscope (Cavaletti, et al., 1992).

2.5 Morphometric assessments in peripheral nerves and DRG

For the morphometric analysis of myelinated fibers, semi-thin sections (1 μm) were observed with a Nikon Eclipse E200 light microscope (Leica Microsystems GmbH, Wetzlar, Germany) at a magnification of 60× and the morphometric analysis was performed using a QWin automatic image analyzer (Leica Microsystems GmbH, Wetzlar, Germany). In randomly selected fields collected from all specimens (section obtained 5 mm from the proximal end), all myelinated fibers evaluable in the analyzed space were counted and the internal (axonal) and external (total) diameters of myelinated fibers were measured, according to previously reported methods on at least 500 myelinated fibers/nerve (Cavaletti, et al., 1992). The histogram of fiber size distribution was calculated and the g-ratio (used as a well-

established measure of the degree of myelination in each fiber assessed from axonal diameter/entire fiber diameter) was automatically calculated. The same blinded observer performed all the morphometric determinations (ACa).
For the morphometric analysis of DRG neurons, 1 μm–thick sections stained with toluidine blue were analyzed with a computer-assisted image analyzer (Image J software, US National Institutes of Health). Serial sections spaced 25 μm were collected and the somatic, nuclear and nucleolar size of DRG sensory neurons were measured on at least 200 DRG neurons/animal in randomly selected sections spaced more than 50 μm as previously described in detail (Canta, et al., 2011). The same blinded observer performed all the morphometric measurements (ACh).

2.6 Intraepidermal Nerve Fiber (IENF) density assessment

At sacrifice hind paw skin specimens were collected. After separating the plantar glabrous skin, which included epidermis and dermis, from the underlying metatarsal bones, 3-mm round samples were taken and immediately fixed in 2% paraformaldehyde-lysine and periodate sodium for 24 h at 4°C, cryoprotected and serially cut with a cryostat to obtain 20 μm-thick sections. Three sections from each footpad were randomly selected and immunostained with rabbit polyclonal anti-protein gene product 9.5 (PGP 9.5; Bio-Rad Company, AbD Serotec) using a free-floating protocol. The same blinded observer (ACh) counted the total number of PGP 9.5-positive IENF in each section under a light microscope 40X magnification with Nikon Eclipse E200 light microscope (Leica Microsystems GmbH, Wetzlar, Germany). Individual fiber were counted as they crossed the dermal–epidermal junction, and secondary branching within the epidermis was excluded. The length of the epidermis was measured using a computerized system (Microscience Inc., Seattle, WA) and the linear density of IENF/mm was calculated (Lauria, et al., 2005).

2.7 Rotating-Polarization Coherent-Anti-stokes-Raman-Scattering (RP-CARS) microscopy of sciatic nerve

Imaging of the samples was performed by means of RP-CARS microscope tuned to the CH_2 vibrational modes. Unfixed sciatic nerves of wild-type mice were frozen at -80°C immediately after the explant and kept at this temperature until the observation. The thawed tissue was put in the central well of a PBS-filled dish (GWSt-3512, WillCo Wells B.V., Amsterdam, The Netherlands) and kept immobilized with a custom-made electrophysiology-type anchor. We observed a total of 5 nerves, belonging to animals aged 1, 5, 12, 23 and 25 months. From each nerve we acquired 4 to 5 z-stacks in different positions along the nerve. Custom-made software (written in Python; Python Software Foundation, Beaverton, OR) was used to analyze the RP-CARS data. The software first selects image areas corresponding to myelin using a

threshold value and then refines this selection by closing the binary mask (Serra,1982). The threshold value was chosen to be the 90th percentile of the A_{dc} signal, i.e. the CARS signal averaged over the rotation of the polarization plane, computed individually from each z-stack. We found this percentile values to be the most appropriate for the thresholding procedure after manual inspection of the generated masks for all the z-stacks, however we have verified that consistent changes of the percentile value do not change significantly the final results.

The software divides each masked image of each z-stack in squared sub-images corresponding to 15 μm x 15 μm in size. This particular size was chosen because we found that in this spatial scale the fiber orientations features are well evident, however we have verified that varying the size up to 50% do not change significantly the final results. For each sub-image the software computes the resultant length β for the φ values of the (N) thresholded pixels, commonly defined as: $\beta = \left| \sum_{j=1}^{N} \exp(i\varphi_j) / N \right|^2$, i. e. one minus the angular variance (Mardia and Jupp, 1999). Finally, the software computes for each z-stack the weighted mean of the resultant lengths from all its sub-images, using the number of masked pixels present in each sub-image as weight.

2.8 Statistical analysis

Data in the text are expressed as mean values ± SD. The differences in nerve conduction studies and morphometry data in DRG, IENF, caudal and sciatic nerves were statistically evaluated at 4 selected time points corresponding to childhood, young adulthood, adulthood and aging (i.e. 1, 7, 15 and 25 month) (Shen, et al., 2011) using the Student's t-test (comparisons month 1 vs. month 7, month 7 vs. month 15, month 15 vs. month 25, Bonferroni's correction with significance level set at $p<0.025$). Correlation between the percentage of fibers larger than 7 μm and NCV or SAP in the caudal nerve was assessed using the linear regression test (Verdú, et al., 2000). The best-fit curve of temporal course of neurophysiological changes was also calculated. These statistical assessments were performed using the Prism 4.0 software (GraphPad Software Inc, La Jolla, CA).

All the statistical computations related to RP-CARS were performed with R software (R Foundation, Vienna, Austria). We averaged the stack-based resultant lengths to obtain animal-based values and then we correlated whose values with the animal age using the Spearman's rank correlation coefficient.

3 RESULTS

3.1 General conditions and toxicity

During the study, no mortality was observed and mice body weight increased along the entire observational period as expected in healthy animals with free access to water and food (from 15.0 g ± 0.17 at 1 month of age to 32.4 g ± 3.44 at 25 months).

At 17, 21 and 25 months of age a slight tendency to increase (still within the age-related normal values) was present in urea (32.0 mg/dl ± 12.1, 40.7 mg/dl ± 7.6 , 44.3 mg/dl ± 12.1), creatinine (0.21 mg/dl ± 0.14, 0.30 mg/dl ± 0.21, 0.90 mg/dl ± 0.72), AST (22.0 mg/dl ± 4.7, 25.7 mg/dl ± 6.7, 43.4 mg/dl ± 18.1) and ALT values (58.5 mg/dl ± 7.2, 55.2 mg/dl ± 5.0, 70.3 mg/dl ± 15.2).

3.2 Nerve conduction studies

The values of caudal and digital NCVs and SAPs obtained at a 2-month interval throughout the observation period are reported in Fig. 1. When the serial values were transposed into a curve they resulted to be best represented by a parabolic function of time (Fig. 1A, 1B, 1C, 1D).

The neurophysiological assessments showed a remarkable increase of caudal NCV (Fig. 1A) from 1 month until t7 months of age, then it remained stable with only a non-significant trend to decrease till the end of the observation period (19.25 m/sec ± 0.98 at 1 month; 31.60 m/sec ± 1.73 at 7 months; 34.09 m/sec ± 2.21 at 15 months; 30.50 m/sec ± 2.70 at 25 months; month 1 vs. month 7: $p < 0.0001$; month 7 vs. 15 and month 15 vs. month 25: p = ns). The same trend was observed for digital NCV, but the decrease observed at the end of the observation period was significant (Fig. 1B) (24.45 m/sec ± 2.89 at 1 month; 29.06 m/sec ± 1.44 at 7 months; 30.76 m/sec ± 1.06 at 15 months; 24.30 m/sec ± 2.1 at 25 months; month 1 vs. month 7: $p < 0.025$; month 7 vs. month 15: p = ns; month 15 vs. month 25: $p < 0.001$).

A significant increase was also present until the animals reached their adulthood in caudal SAP (Fig. 1C) then it remained stable with a significant decrease at the end of the observation period (50.4 μV ± 9.63 at 1 month; 125.0 μV ± 16.36 at 7 months; 127.0 μV ± 8.96 at 15 months; 107.9 μV ± 5.45 at 25 months; month 1 vs. month 7: $p < 0.0001$; month 7 vs. month 15: p = ns; month 15 vs. month 25: $p < 0.01$). The same course was observed for digital SAP (Fig. 1D) (100.0 μV ± 57.86 at 1 month; 337.7 μV ± 123.2 at 7 months; 203.1 μV ± 34.38 at 15 months; 122.1 μV ± 27.9 at 25 months; month 1 vs. month 7: $p < 0.001$; month 7 vs. month 15: p = ns; month 15 vs. month 25: $p < 0.01$).

3.3 Light and electron microscopy of caudal nerve

Representative images of caudal nerve sections obtained from animals at different time points are reported in Supplementary Fig. 1. The morphological assessment performed at the light microscope demonstrated that the nerve structure at 1 month of age was still immature and progressive increase in size was evident in myelinated fibers during nerve maturation (Supplementary Fig. 1A, 1D, 1G, 1L). This increase in fiber size was paralleled by a reduction of fiber density, as confirmed by the morphometric assessment (see below). Ultrastructural observations revealed that, although already at 1 month of age the myelin sheath was overall already well organized, a few small diameter fibers still had a thin myelin sheath if compared with axonal size (Supplementary Fig. 1B, 1C). Several Schwann cells observed at the age of 1 month had an activated aspect, with enlarged cytoplasm and increased number of intracytoplasmic organelles (Supplementary Fig. 1C). These ultrastructural features were no longer present in the adult caudal nerve (Supplementary Fig. 1E, 1F, 1H, 1I), although rare Schwann cells still maintained an activated aspect. When the aged nerves (25 months) were examined, a decrease of myelinated fibers density was evident at the light microscope (Supplementary Fig. 1L). The ultrastructural examination demonstrated that axons maintained a normal aspect (Supplementary Fig. 1M, 1N). By contrast, the occurrence of myelin infoldings and outfoldings, only occasional until 7 months of age, became particularly evident in the largest myelinated fibers and their presence progressively increased (15 months, Supplementary Fig. 1H, 1I) until the end of the observation period, sometimes with the appearance of intra-axonal myelin ovoids (Supplementary Fig. 1M, 1N). Similarly, myelinated fibers with uncompacted myelin lamellae were observed. Occasionally, myelin debris were observed in the cytoplasm of myelinating Schwann cells in the nerves of aged mice (Supplementary Fig. 1N). The morphological aspect of unmyelinated fibers and of endoneural vessels was substantially unchanged along the entire period of observation, with only rare duplications in the basal membrane in a few endoneural vessels. Age-related increase in the frequency of denervation bands (i.e. Schwann cell profiles not surrounding at least one axon) was observed, in agreement with the reduction in nerve fibers density (see below). Endoneural collagen, fibroblasts and perineural cells maintained a normal aspect along the entire period of observation.

3.4 Morphometric analysis of caudal nerve

The results of caudal nerve morphometric analysis performed on specimens obtained every 2 months are graphically summarized in Fig. 2. As shown in Fig 2A, during the course of the study the myelinated fiber density had remarkable

changes, with higher values at the first month of age, followed by a marked decrease due to physiological nerve maturation and axonal sorting. From the third month of age, caudal fiber density steadily decreased till the end of the observation period (2239 fibers/μm^2 ± 200.2 at month 1; 1610 fibers/μm^2 ± 169.6 at month 3; 1494 fibers/μm^2 ± 126.2 at month 7; 1345 fibers/μm^2 ± 111.1 at month 15; 1025 fibers/μm^2 ± 121.7 at 25 months; month 1 vs. month 7: $p < 0.0001$; month 7 vs. month 15: $p < 0.025$; month 15 vs. month 25: $p < 0.0001$), with a sudden drop in myelinated fibers density after the age of 21 months. The axonal size of myelinated fibers significantly increased in the maturation phase (month 1 = 3.790 μm ± 0.83; month 7 = 5.570 μm ± 1.21; $p<0.0001$), then it remained substantially stable until the end of the observation period (month 15 = 5.851 μm ± 1.36; month 25 = 5.929 μm ± 1.75; p = ns). By contrast, g-ratio values (Fig. 2B) were significantly different at month 1 and month 25 vs. months 7 and month 15 (0.72 ± 0.08 at month 1; 0.80 ± 0.06 at month 7; 0.81 ± 0.05 at month 15; 0.77 ± 0.10 at month 25; month 1 vs. month 7: $p < 0.0001$; month 7 vs. month 15: p = ns; month 15 vs. month 25: $p < 0.0001$), with a higher value in adulthood vs. both childhood and aging. The analysis of the fiber size distribution (Fig. 2C) showed unimodal distribution with a progressive shift to larger fiber diameter with maturation and aging.

When the morphometric results obtained at sacrifice were plotted against the neurophysiological results to assess their correlation, it resulted that the caudal NCV and SAP data represent a linear function of the percentage of fibers with diameter larger than 7 μm (Supplementary Fig. 2A, 2B).

3.5 Light and electronic microscopy of sciatic nerve

Representative images of sciatic nerve sections obtained from animals at different time points are reported in Fig. 3. Although the myelinated nerve fibers profiles were overall more regular, most of the morphological aspects described in the caudal nerve could also be observed in the sciatic nerve, as expression of maturation and aging. In particular, progressive increase in the occurrence of myelin irregularities and reduction in the density of myelinated fibers were evident. In addition to these changes, rare fibers undergoing active axonal degeneration were present in the specimens collected at the end of the 2-year observation period (Fig. 3N), in association with Schwann cells bearing intracytoplasmic vacuolation (Fig. 3M, 3N, 3O, 3P). The unmyelinated fibers maintained a normal aspect also in the sciatic nerve and endoneural vessels very rarely had mild duplications in the basal membrane. Denervation bands

increased with aging, while endoneural collagen, fibroblasts and perineural cells maintained a normal aspect along the entire period of observation.

3.6 Morphometric analysis of sciatic nerve

The results of sciatic nerve morphometric analysis performed on specimens obtained every 2 months are graphically summarized in Fig. 2. Changes in myelinated fiber density were observed also in the sciatic nerve (Fig. 2D), with higher values at the first month of age, followed by a marked decrease during the observation period. As observed in the caudal nerve, the myelinated fiber density steadily decreased from the third month of age till the end of the observation period (2296 fibers/μm^2 ± 226.4 at month 1; 1659 fibers/μm^2 ± 136.8 at month 3; 1628 fibers/μm^2 ± 181.2 at month 7; 1355 fibers/μm^2 ± 182.5 at month 15; 1307 fibers/μm^2 ± 177.8 at month 25; month 1 vs. month 7: $p < 0.0001$; month 7 vs. month 15: $p < 0.01$; month 15 vs. month 25: p = ns). The axonal size of myelinated fibers significantly increased in the maturation phase (month 1 = 3.945 μm ± 1.01; month 7 = 5.375 ± 1.937, $p<0.0001$), then it remained substantially stable until the end of the observation period (month 15 = 5.993 ± 1.846; month 25 = 5.450 μm ± 2.15, p = ns). G-ratio values (Fig. 2E) were significantly different at month 1 and month 25 vs. months 7 and 15 (0.69 ± 0.06 at month 1; 0.77 ± 0.05 at month 7; 0.77 ± 0.05 at month 15; 0.70 ± 0.09 at month 25; month 1 vs. month 7: $p < 0.0001$; month 7 vs. month 15: p = ns; month 15 vs. month 25: $p < 0.0001$), with the same course observed in the caudal nerve. The variation in the myelinated fiber size along the observation period confirmed in the sciatic nerve that an evident shift toward larger fibers occurred with maturation and aging as observed in the caudal nerve (Fig. 2F). The size distribution was clearly unimodal at the youngest ages, then it became bimodal in adulthood with a trend toward return to unimodality and decrease of the percentage of the largest myelinated fibers with aging.

3.7 RP-CARS on sciatic nerve

The employed RP-CARS setup allows the detection of the average in-plane orientation and the degree of anisotropy of the CH_2 bonds inside the excitation point spread function-volume (de Vito, et al., 2012,de Vito, et al., 2014). The vast majority of CH_2 bonds inside the myelin walls are aligned, on average, parallel to the myelin sheath. Therefore, RP-CARS allows not only the identification of the sheaths (a CARS image of myelinated axons in a mouse sciatic nerve is shown in Fig. 4A, where light areas represent high concentrations of CH_2 bonds and therefore identify myelin sheaths), but also the determination of their local orientation with sub-micrometric resolution. Exploiting the planned data-analysis

pipeline, from the RP-CARS raw data we quantified for each acquisition the resultant length β of the myelin sheath orientations over a chosen spatial scale. As depicted in Fig. 4D, we have found in the sciatic nerve, on a micrometric spatial scale, a significant ($p < 0.05$) decrease of β with respect to the animal age (Spearman correlation coefficient: -0.9), i.e. an increase of the spatial disorder of the sheath local orientation. In particular, the 25 month old-mouse resultant length was significantly decreased when compared to younger mice (1, 5 and 13 months; $p < 0.01$ in all comparisons). This finding is rendered easily visible by color-mapping the φ values as depicted in Figs. 4B and 4C, which shows representative cases of the 1-month and 25-month old mice, respectively. The "banded" appearance of the myelin walls belonging to the older mouse implies frequent variation of the local orientation of the myelin sheaths.

3.8 IENF density assessment

IENF density was serially assessed along the study period and the results are graphically summarized in Fig. 5. The morphometric assessment showed a steady decrease in the IENF density, which became particularly evident after the age of 17 months and was striking at 23 and 25 months of age (49.6 ± 3.7 IENF/mm at month 1; 42.9 ± 7.6 IENF/mm at month 7; 38.2 ± 1.5 IENF/mm at month 15; 17.7 IENF/mm ± 3.6 at month 25; month 1 vs. month 7: p = ns; month 7 vs. month 15: p = ns; month 15 vs. month 25: p <0.0001). The morphological aspect of the IENF was normal, despite a reduction in their density (Fig. 5B).

3.9 Morphological and morphometric evaluation of DRG

The morphological aspect at the light and electron microscope of the DRG neurons and satellite cells remained substantially unchanged until the animals reached the age of 15 months. In the subsequent period, vacuolation of satellite cells cytoplasm became apparent (Fig. 6A, 6B), and their incidence increased with age, occasionally forming large vacuoles occupying the entire cytoplasm (Fig. 6C). Moreover, dark inclusions with a lamellar aspect were frequently observed in the cytoplasm of satellite cells (Fig. 6A, 6B, 6D). In the DRG neurons the incidence of intracytoplasmic electrondense inclusions progressively increased with age and they assumed a lipofuscin-like aspect (Fig. 6D). Neurons with a condensed aspect of the cytoplasm were also present in aged mice, although their occurrence was rare (Fig. 6A). The serial morphometric assessment performed on the soma, nucleus and nucleolus of the DRG neurons (Fig. 6E, 6F, 6G) did not evidence any significant change in the somatic and nuclear size. By contrast, a significant increase in the size of the nucleolus was observed in aged mice (month 1 = 5.683 μm^2 ± 3.17; month 7 =

5.082 μm^2 ± 2.64; month 15 = 5.468 μm^2 ± 2.84; month 25 = 6.306 μm^2 ± 3.11; month 1 vs. month 7: $p < 0.001$; month 7 vs. month 15: $p < 0.025$; month 15 vs. month 25: $p < 0.0001$). This increase in nucleolar size was associated at the ultrastructural level in aged mice to evident segregation of the granular and fibrillar components in a proportion of neurons.

4 DISCUSSION

In animal models, the effect of aging on the peripheral nervous system has been investigated in a few studies (Ceballos, et al., 1999,Jeronimo, et al., 2008,Melcangi, et al., 2003,Shen, et al., 2011,Verdú, et al., 1996,Verdú, et al., 2000) which reported structural changes in the peripheral nerves at the biochemical and pathological levels. These changes were corroborated by functional impairment as slowing in NCV as well as reduction in nerve SAP (Shen, et al., 2011,Verdú, et al., 2000). However, despite age-related sensory changes can be the result of a damage at any level of the peripheral sensory pathway, these studies investigated only the trunks of the nerves without assessing changes in the DRG primary sensory neurons or in the distal innervation. In this regard it must be noted that the skin nerve fibers density is a pathologic readout potentially applicable also to trials in humans and not investigated longitudinally in previous animal studies.

Since the importance of collecting reliable data on the peripheral nervous system changes in aging animals has been so far underestimated, this study fills a gap in the preclinical knowledge of a condition with remarkable effects on the quality of life of otherwise healthy elderly persons and also have important impacts at the socio-economic level.

In our 2-year longitudinal study in C57BL/6 mice we investigated the effects of aging applying morphologic/morphometric methods on the DRG, peripheral nerves and skin innervation and in parallel we assessed the neurophysiological changes occurring in the digital and caudal nerves. Our observations were carried out for the first time on the same cohort of mice housed at the age of 1 month and allowed to grow until 25 months, thus excluding differences due to the features of different cohorts of animals. Moreover, since it was previously observed that myelin changes are prominent with aging (Melcangi, et al., 2003,Melcangi, et al., 1998), we performed an advanced analysis of myelin structure with a highly sensitive method such as RP-CARS in order to detect possible submicroscopic changes and to assess their timing.

Continuous assessment of the general conditions and blood chemistry analysis evidenced that at 25 months of age our mice underwent physiologic aging and the observed changes in the PNS functioning and structure were therefore age-related and not due to any concomitant diseases. This observation allows to consider these animals at the end of the study as the counterpart of healthy aged persons, since based on the typical life span of C57BL/6 mice, 25 months of age correspond to 70-80 years of age in humans (Dutta and Sengupta, 2015).

Further confirmation of the reliability of our animal model of PNS aging is provided by the course of the neurophysiological changes observed in the study, which were consistent with peripheral nerve myelinated fibers maturation in the earliest months, followed by stabilization in NCV and SAP values and eventually showing a trend toward the reduction in both parameters as described in humans (Bouche, et al., 1993). The changes in both NCV and SAP in the caudal and digital nerves were represented by a parabolic curve, in agreement with the data obtained using a different recording method by Verdù et al. (Verdú, et al., 1996,Verdú, et al., 2000) for NCV. Technical differences in the methods used to record potential amplitudes in that study prevent a comparison with our SAP data. This parabolic course of the neurophysiological changes is explained by the detailed observations reported by Ceballos et al. (Ceballos, et al., 1999) showing that most of the changes in the structure of the peripheral nerves are non-linear, as confirmed also by Verdù et al. (Verdú, et al., 2000) and by the morphometric results of our study.

Taken together our data indicate that in the peripheral nervous system physiological modifications occur during senescence and all the parameter examined show coherent changes.

At the pathological level, light microscope observations and morphometry provided structural evidence for these neurophysiological changes. The density of myelinated fibers which was very high at 1 month of age sharply decreased since the beginning of the second month and this reduction was paralleled by an increase of myelinated fibers size and increased thickness of the myelin sheath, two events closely related to nerve maturation (Shen, et al., 2011). With aging, the density of myelinated fibers slightly and progressively decreased until the age of 21 months when, particularly in the caudal nerve, a more marked decrease in the density of myelinated fiber occurred, in agreement with previous studies (Ceballos, et al., 1999,Verdú, et al., 2000). The hypothesis that this decrease is simply apparent and secondary to axonal atrophy (Ceballos, et al., 1999) is not confirmed by our direct morphometric assessment. The correlation

analysis allows to confirm the relationship existing between the percentage of large myelinated fibers in the sciatic nerves and neurophysiological changes, as obtained in other peripheral nerves in mice (Shen, et al., 2011).

The ultrastructural examination evidenced that at 1 month of age, Schwann cells had the typical activated aspect occurring during nerve maturation as well as in regeneration (Komiyama and Suzuki, 1992,Tanaka, et al., 1992) and that a proportion of fibers (particularly those of relatively small size) still had a thin myelin sheath if compared with the axonal size. These features were no longer present in the mature nerve and the morphological features of nerve fibers remained unchanged until the age of 15 months, when irregularity of myelin (lamellae separation, myelin loops, in- and outfoldings) appeared (Knox, et al., 1989). These changes which have also been associated with concomitant axonal damage, as well as denervation bands and collagen pockets (Ceballos, et al., 1999,Krinke, et al., 2014) were more frequent in the oldest mice and in the caudal nerve. The higher incidence of myelin irregularities in the caudal vs. the sciatic nerve observed in our study very closely mimics the human condition where a distal-to-proximal gradient of nerve impairment occurs. Although well-characterized myelin changes have been described at the morphological level in aged animals (Ceballos, et al., 1999,Shen, et al., 2011), the occurrence of biochemical alterations in myelin proteins even at younger ages (Melcangi, et al., 2003,Melcangi, et al., 1998) raises the possibility that more subtle myelin abnormalities could be evident also in normally-appearing myelinated fibers in aged mice.

RP-CARS has been used for the first time in this study to investigate age-related changes. CARS imaging is an advanced imaging method based on chemical contrast: the energy difference of two excitation (pump and stokes) photons matches the energy of one of the vibrational mode of the target system, e.g. CH_2 bonds. A third photon (probe) probes these coherently excited vibration modes. The system then relaxes to the ground state emitting the CARS photons. By means of a recent development of CARS microscopy, RP-CARS (de Vito, et al., 2012), using a rotating pump polarization plane it is possible to visualize the degree of anisotropy in bond alignment and to detect their average orientation direction (φ) within the sub-micrometric excitation volume of the RP-CARS microscope (de Vito, et al., 2015). This technique represents an ideal tool to investigate changes in a structure like myelin, being healthy myelin characterized by a high degree of molecular order (de Vito, et al., 2015). The RP-CARS data showed a decrease of the resultant length with aging in the myelin sheath orientations on a micrometric spatial scale in the sciatic nerve. This observation can be interpreted as the onset of a “varicosity” in the myelinated nervous fibers in older animals.

Compared to the g-ratio that in young mice increases up to the 7th month, the β value appears to be constant. On the other hand, at later ages, both the g-ratio and the β value decrease. This comparison suggests an intriguing hypothesis: that the g-ratio alterations occurring during the early age of the animals could be of different nature with respect to the ones observed during the advanced age; the first not being associated with a state of myelin alteration (i.e. an effect of the developmental maturation of the nervous system), differently from the second (i.e. an effect of aging). We argue that this observed varicosity could be one of the causes, along with possible subtle abnormalities in the myelin composition and/or in the axon ionic channel expression and modulation, at the basis of the measured decrease in the sensory/motor NCV in older animals.

When myelin features were investigated at the morphometric level with the classical light microscopic approach, an inverted U-shaped distribution of the g-ratio was observed in both sciatic and caudal nerves. This result is in apparent conflict with the data reported in mice by Ceballos et al. (Ceballos, et al., 1999), since they reported that myelin thickness slightly decreases between 12 and 20 months of age for all axon sizes, then tended to increase with increasing age, particularly in small diameter fibers. However, the same Authors recognized that the discrepancy between direct measurement of myelin thickness and the g-ratio results (which are more commonly used in the clinical assessment of nerve biopsies and for this reason has been selected as myelination indicator in our study) might be due to apparent increase in those fibers with uncompacted myelin lamellae leading to over-estimation of the actual thickness. Moreover, it is very likely that a specific pattern for the dynamics of the g-ratio exist in each peripheral nerve (Fahrenkamp and Friede, 1987) and that differences may be marked even among species and at different time points of observations. For instance, while Jeronimo et al. (Jeronimo, et al., 2008) and Soltanpuor et al. (Soltanpour, et al., 2012) observed clear-cut changes in the g-ratio in the hypoglossal and sural nerves of rats, Chentanez et al. (Chentanez, et al., 2010) did not observe any change in the superficial branch of the radial nerve. No animal study reproduced the time course and the severity of the changes reported by Jacobs and Love (Jacobs and Love, 1985) in human sural nerves, where the g-ratio remained stable around a value of 0.65 until the age of 60, then it progressively increased until a final value close to 1.

Regarding skin innervation, steady decrease in IENF density was observed with aging in mice, a result in complete agreement with the reduction reported in humans (Lauria, et al., 2010). This information is particularly relevant, since

IENF is gaining increasing interest as a reliable pathological readout in clinical trials and correlation between skin innervation, neurophysiological changes and peripheral neuropathy has been reported in animal models (Bianchi, et al., 2004,Lauria, et al., 2005).

While several of the observations described in our mice study can be correlated with data obtained in aging persons, very few data are available regarding age-related changes in DRG primary sensory neurons and nearby satellite cells in humans (Schmidt, et al., 1997). We did not observe generalized degeneration in neurons or satellite cells at any age, but clear age-related changes were anyway present in both cell populations in aged mice (Schmidt, et al., 1997), and when they occurred they were severe. Intracellular inclusions with different morphological aspects increased with age and they were much more evident in 25-month old mice than in animals of younger age, particularly in satellite cells. These features were described as being limited to neurons in a previous study in mice, but the observations were performed only at the light microscope (Krinke, et al., 2014). Nucleolar segregation of the granular and fibrillar components of the nucleolus was a feature in several primary neurons and this might contribute to the observed increase in nucleolar size in aged mice.

5 CONCLUSION

Overall, our data allow to draw a functional and pathological description of the changes occurring in healthy aging mice and they reflect the expected course of PNS aging in humans. Our results are in substantial agreement with previously reported studies performed in animals up to the age of 33 months (Ceballos, et al., 1999,Shen, et al., 2011), but they add significant new data and have the peculiarity to allow a direct comparison between a large set of investigational methods in mice at the same age and along the entire 2-year study. Therefore, our data might provide the background for mechanistic studies designed to investigate on possible pathophysiological events at the basis of the observed age-related changes in healthy mice PNS allowing the selection of the most appropriate time points and readouts according to the investigation aims. Moreover, the identification of the course of PNS changes in young, adult and aging mice might allow to study the effect of experimentally-induced disease-related changes (e.g. diabetes, drug-induced, traumatic) on the PNS, currently investigated in young animals despite their common occurrence in aged in humans.

Figures

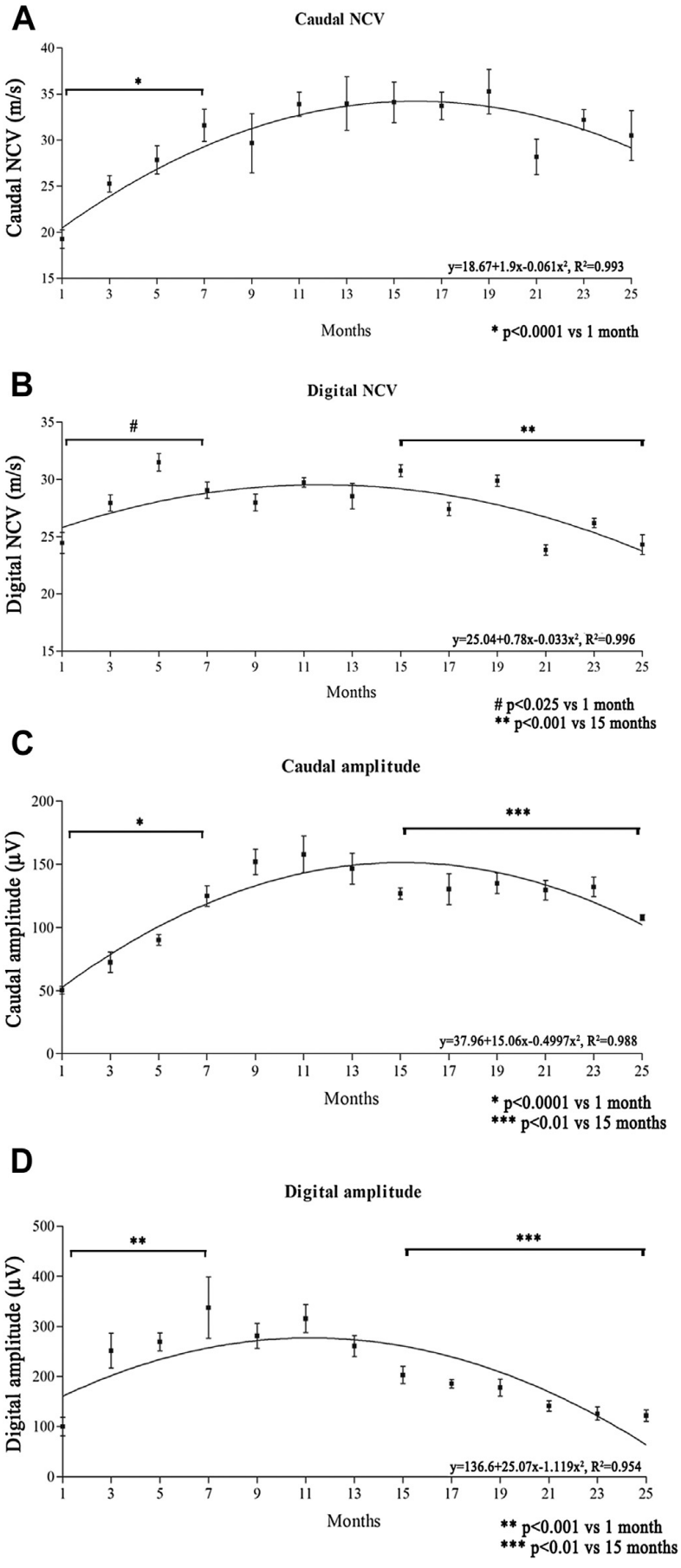
A
Caudal NCV
Caudal NCV (m/s)
y=18.67+1.9x-0.061x², R²=0.993
Months
* p<0.0001 vs 1 month
B
Digital NCV
Digital NCV (m/s)
y=25.04+0.78x-0.033x², R²=0.996
Months
# p<0.025 vs 1 month
** p<0.001 vs 15 months
C
Caudal amplitude
Caudal amplitude (µV)
y=37.96+15.06x-0.4997x², R²=0.988
Months
* p<0.0001 vs 1 month
*** p<0.01 vs 15 months
D
Digital amplitude
Digital amplitude (µV)
y=136.6+25.07x-1.119x², R²=0.954
Months
** p<0.001 vs 1 month
*** p<0.01 vs 15 months

Figure 1: time course of the neurophysiological changes observed in the 2-year period of observation in caudal and digital nerves (A, B = nerve conduction velocity, NCV; C, D = nerve potential amplitude). Comparison between the results obtained at month 1 of age vs. month 7, month 7 vs. month 15 and month 15 v. month 25 are reported when significant. Best fitted parabolic function of time of the observed neurophysiological results are indicated in each panel.

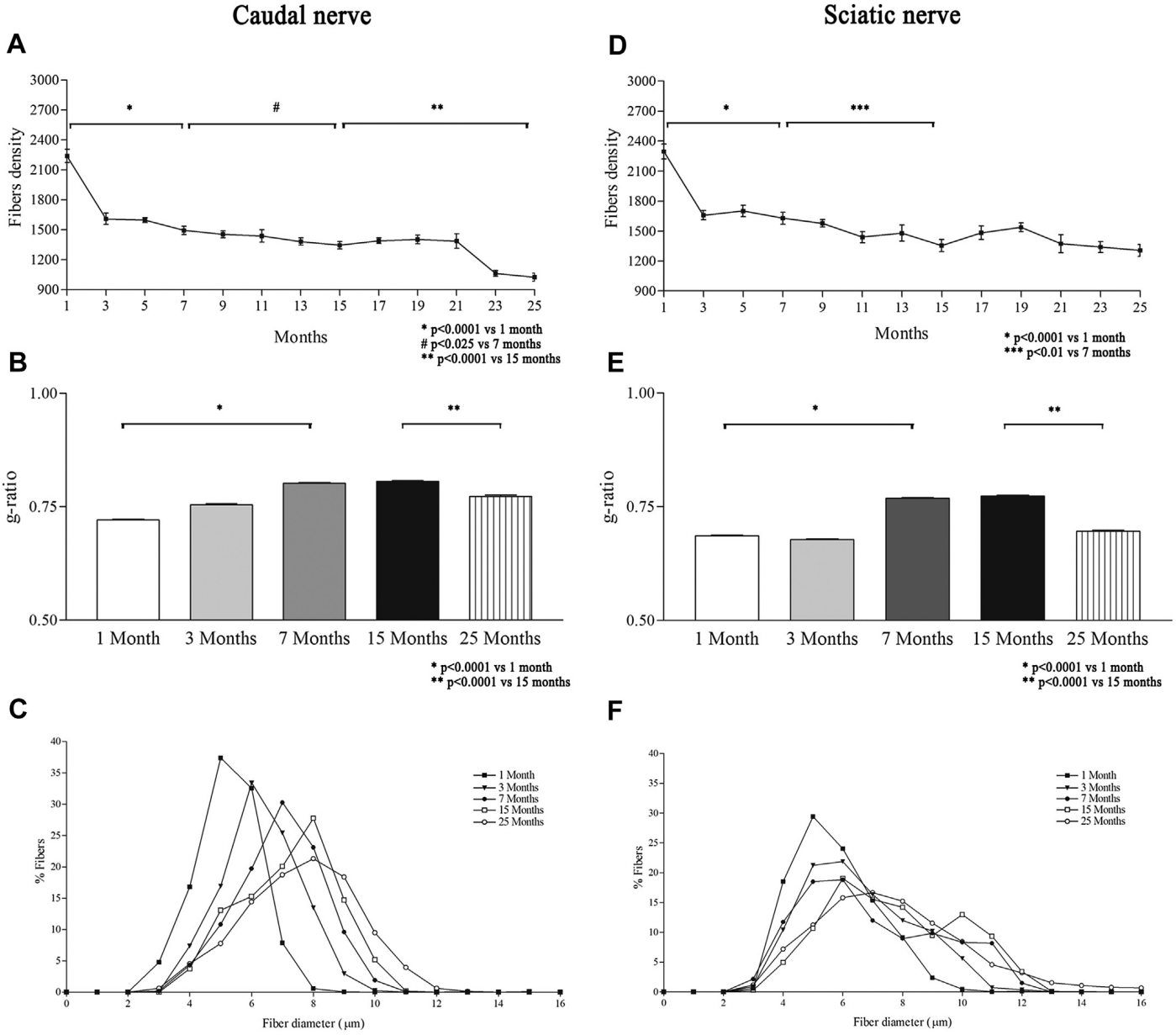

Figure 2: Morphometric assessments in the caudal (A-C) and sciatic nerves (D-F). Comparison between the results obtained at month 1 of age vs. month 7, month 7 vs. month 15 and month 15 v. month 25 are reported when significant in panels A, B, D and E. The frequencies of myelinated fibers according to their external diameter are reported in C and F.

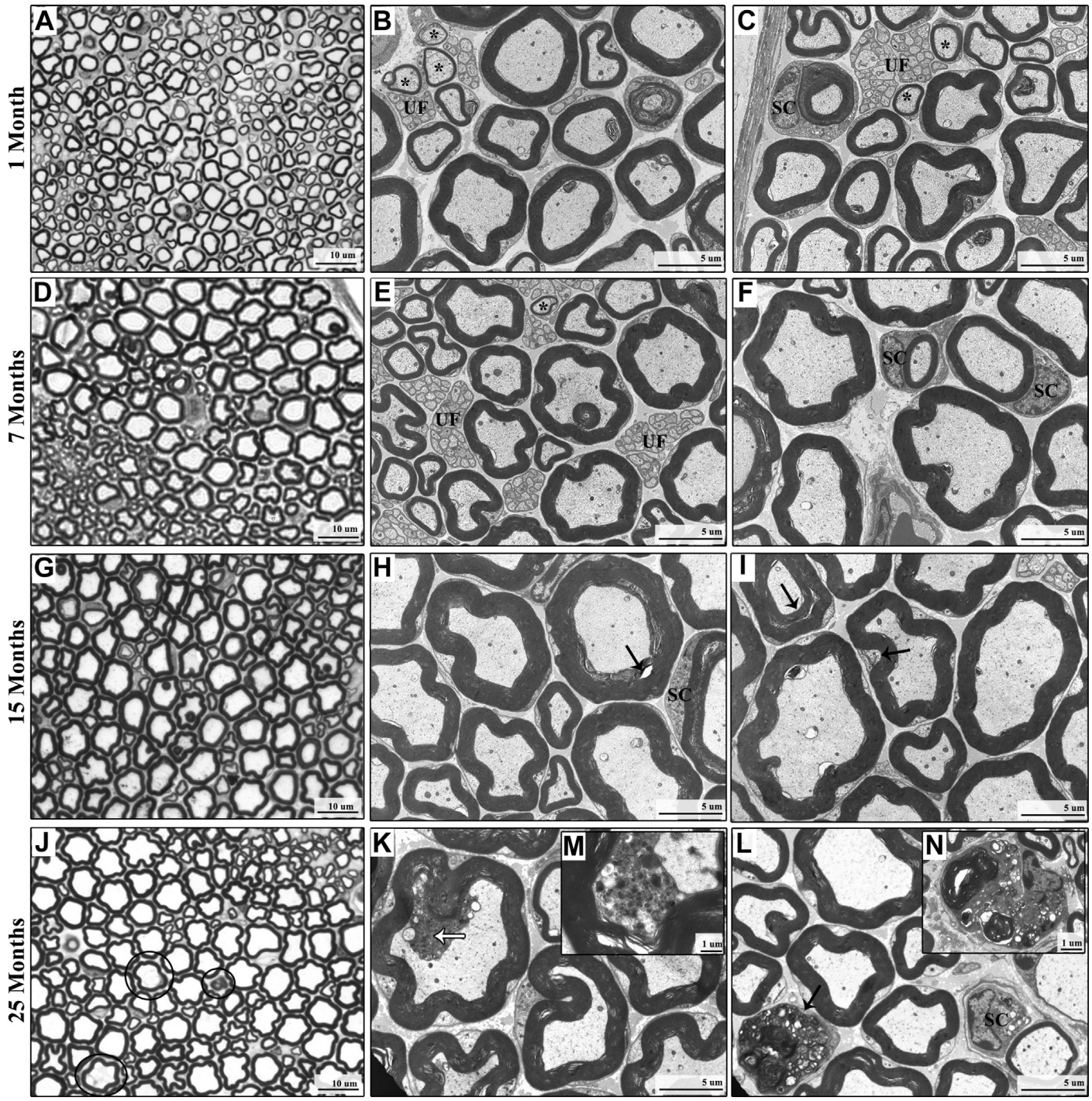

Figure 3: Representative images of sciatic nerve sections obtained from animals at different ages. As evidenced at the light microscope in the caudal nerve, also in the sciatic nerve maturation of the myelinated fibers is evident from month 1 of age (A) to months 7, 15 and 25 (D, G, L). Fibers with thin myelin are more frequent in young mice (asterisk, B,C), then myelin irregularities start to become evident (E, F) and they become frequent with aging (black arrows, H, I, M, N). In addition to these changes, rare fibers undergoing active axonal degeneration are shown in the nerves collected at the

end of the 2-year observation period (circle, L; black arrow, N, P). Moreover, Schwann cells (SC) bearing intracytoplasmic vacuolation occur exclusively in aged mice (M, white arrow, N, O). The unmyelinated fibers (UF) have a normal aspect.

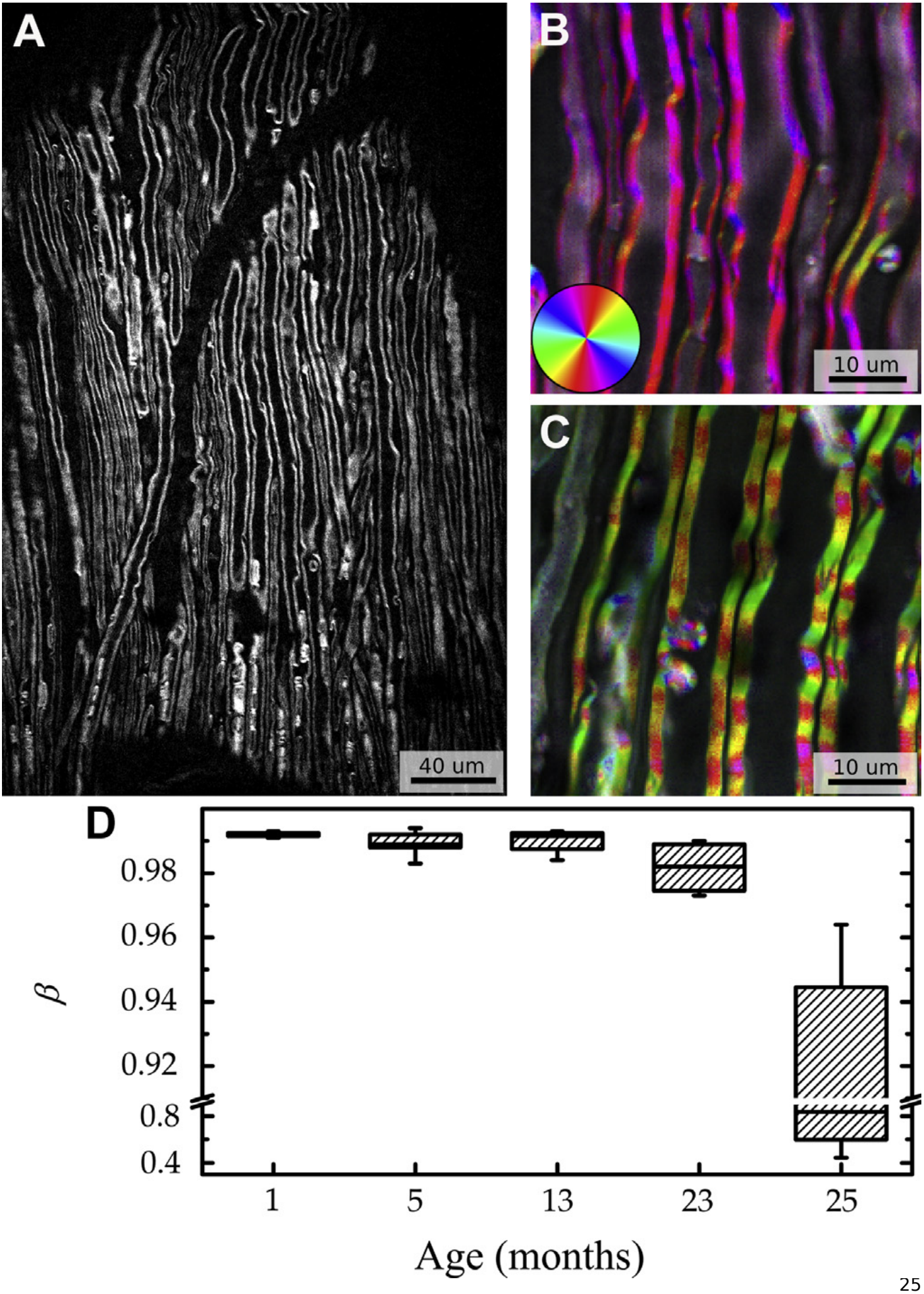
A
40 um
B
10 um
C
10 um
D
0.98
0.96
0.94
0.92
0.8
0.4
β
1
5
13
23
25
Age (months)

Figure 4: RP-CARS analysis of sciatic nerves. (A) Representative RP-CARS image of a portion of sciatic nerve from a 1-month old mouse. Myelin sheaths, sectioned by the optical imaging plane, appear in white thanks to the high concentration of CH_2 bonds. The scale bar corresponds to 40 μm. (B) Color-coded RP-CARS image of a 1-month-old-mouse sciatic nerve. Colors indicate different average orientations of the CH_2 bonds (scale bar: 10 μm). (C) Color-coded RP-CARS image of a 25-month-old-mouse sciatic nerve. Colors and scale bar as in Panel b. (D) Analisys of the average angular dispersion (β) as a function of mice age.

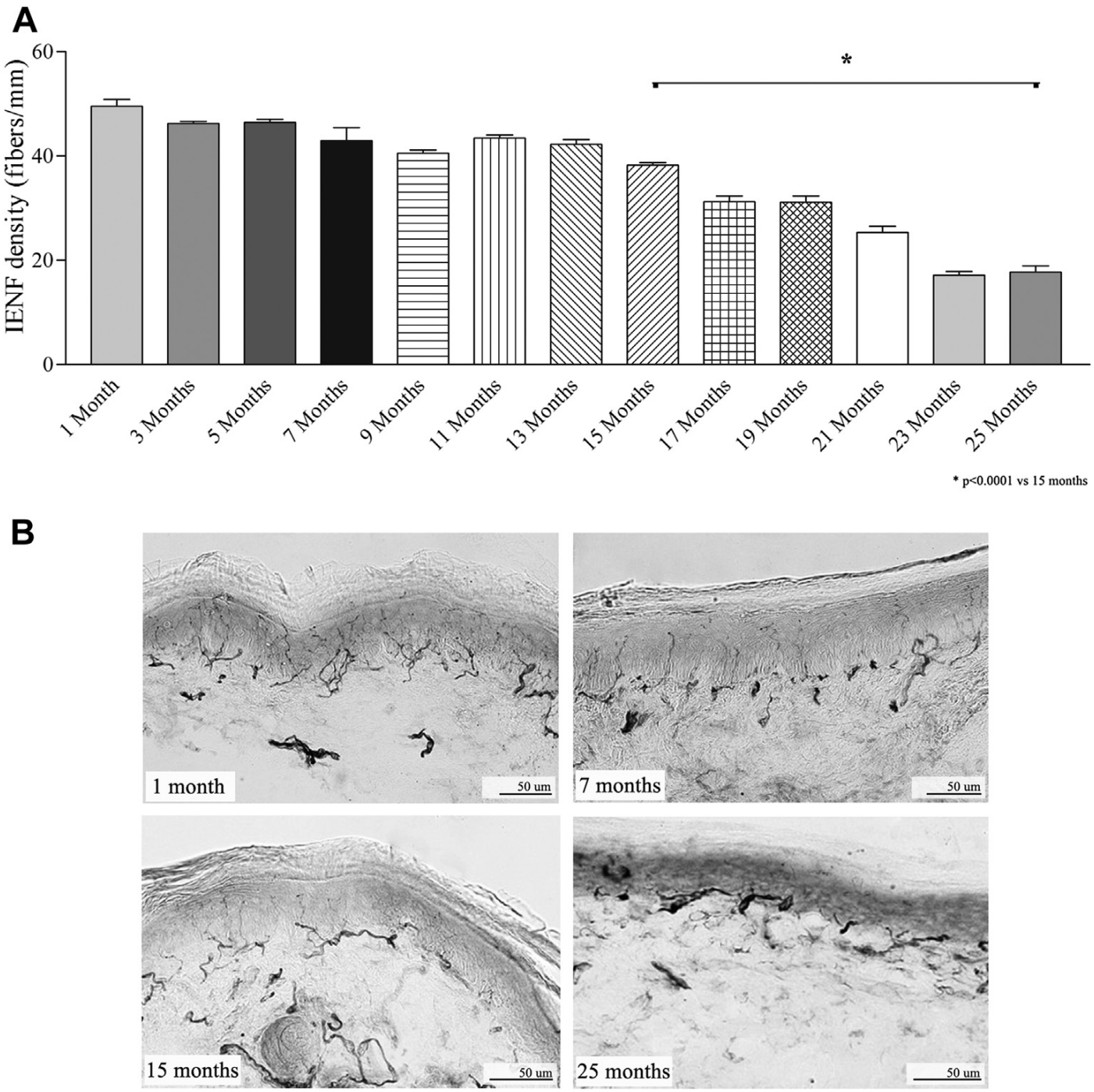

Figure 5: Longitudinal assessment of intraepidermal nerve fiber density (IENF) in the footpad (A). Comparison between the results obtained at month 1 of age vs. month 7, month 7 vs. month 15 and month 15 v. month 25 are reported when significant. Despite evident reduction in their density, the morphologic aspect of the remaining fibers is preserved along the entire period of observation, as shown by the images taken at different ages (B).

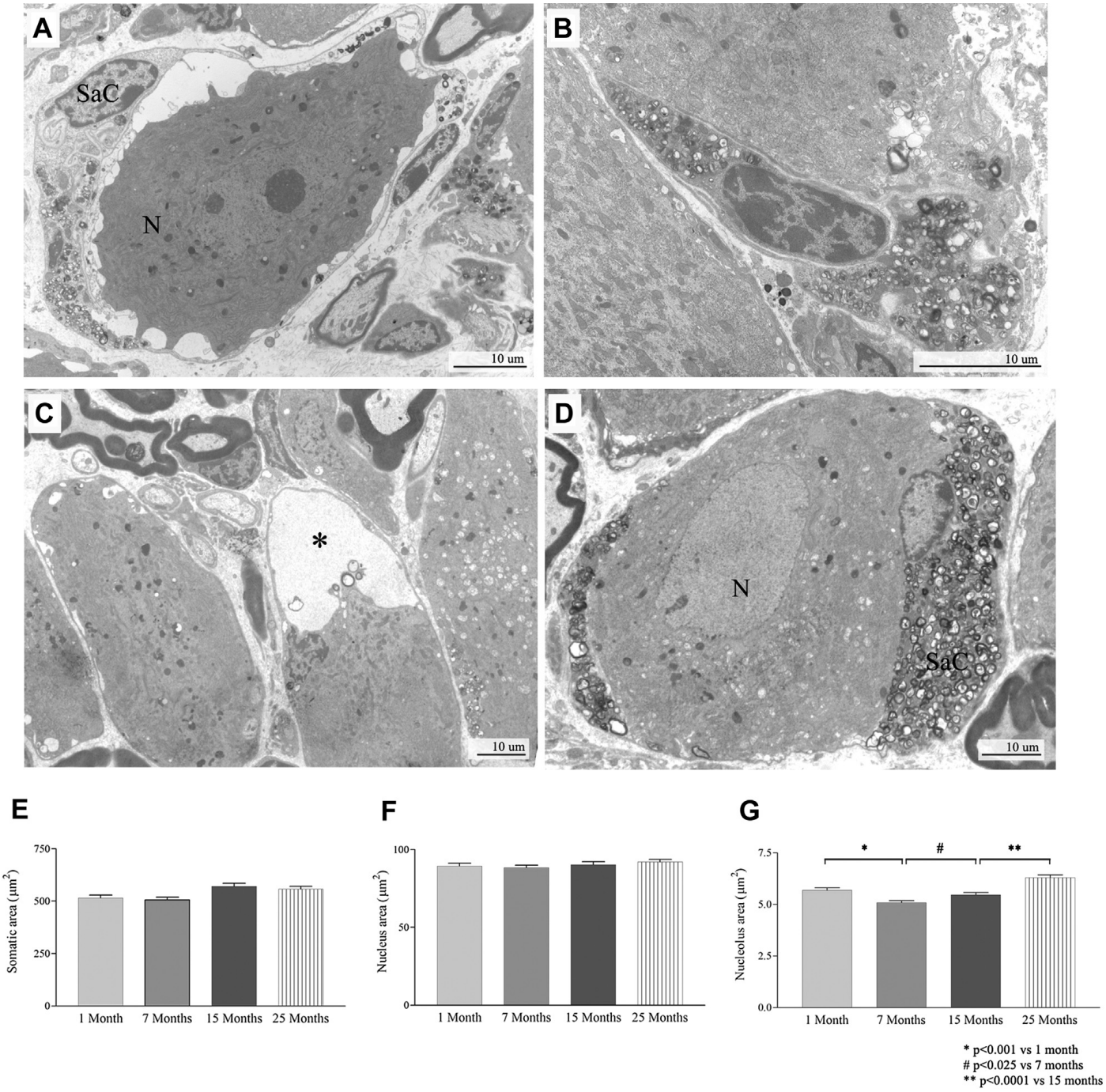

Figure 6: Representative electronmicrographs of dorsal root ganglia (DRG) obtained from 25-month old mice. Vacuolation of satellite cells (SaC) cytoplasm is evident (A,B), occasionally forming large vacuoles occupying the entire cytoplasm (asterisks, C). Dark inclusions with a lamellar aspect are shown in the cytoplasm of satellite cells (A,B,D). In the DRG neurons (N) the incidence of intracytoplasmic electrondense inclusions increased with age and they assumed a lipofuscin-like aspect (D). Neurons with a condensed aspect of the cytoplasm were also present in aged mice, although their occurrence was rare (A). The serial morphometric assessment performed on the soma, nucleus and

nucleolus of the DRG neurons (E-F) did not evidence any significant change in the somatic and nuclear size, while a significant increase in the size of the nucleolus was observed in aged mice. Comparison between the results obtained at month 1 of age vs. month 7, month 7 vs. month 15 and month 15 v. month 25 are reported when significant.

Supplementary Figures:

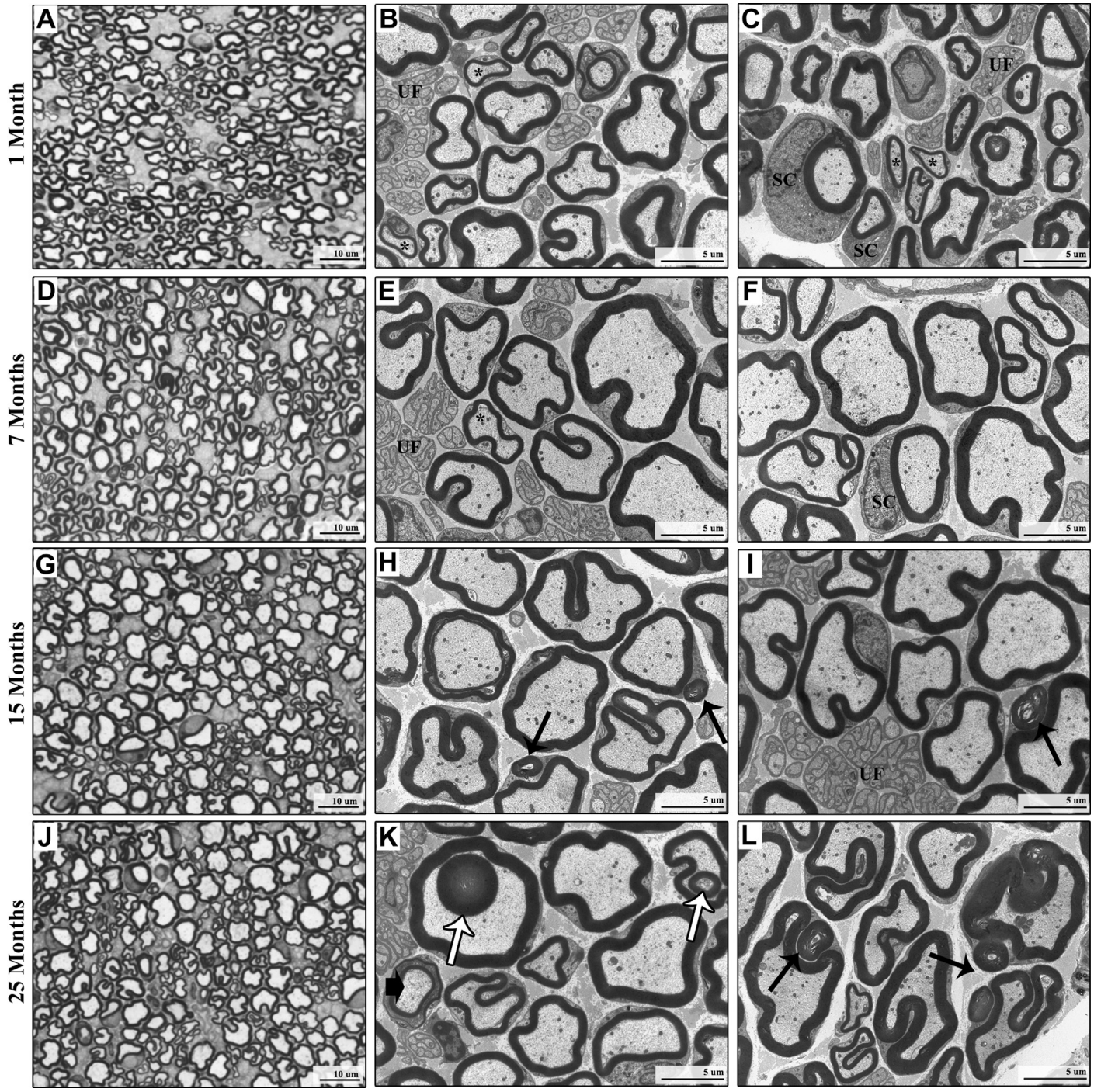

Supplementary Figure 1: Light (A, D, G, J) and electron microscope (B, C, E, F, H, I, K, L) representative images of caudal nerve samples at the age of 1, 7, 15 and 25 months. At the light microscope the nerve structure appears immature at the age of 1 month and progressive increase in size with reduction in fiber density occurs in myelinated fibers during maturation of the nerve (Supplementary Fig. 1A, 1D, 1G, 1J). At the ultrastructural observation a few small diameter fibers still had a thin myelin sheath if compared with axonal size at 1-month age (asterisks, Supplementary Fig.

1B, 1C) and several Schwann cells (SC) have an activated aspect (Supplementary Fig. 1C). In the aged nerves, axons maintained a normal aspect (Supplementary Fig. 1K, 1L), while the occurrence of myelin infoldings and outfoldings, only occasional until 7 months of age, becomes particularly evident in the largest myelinated fibers and their presence progressively increases (Supplementary Fig. 1H, 1I) until the end of the observation period. Myelin ovoids are also evident in the axonal space in 25-month old mice (white arrows, Supplementary Fig. 1K, 1L). Occasionally, myelin debris are present also in the cytoplasm of myelinating Schwann cells in the nerves of aged mice (black arrows). The unmyelinated fibers (UF) have a normal aspect.

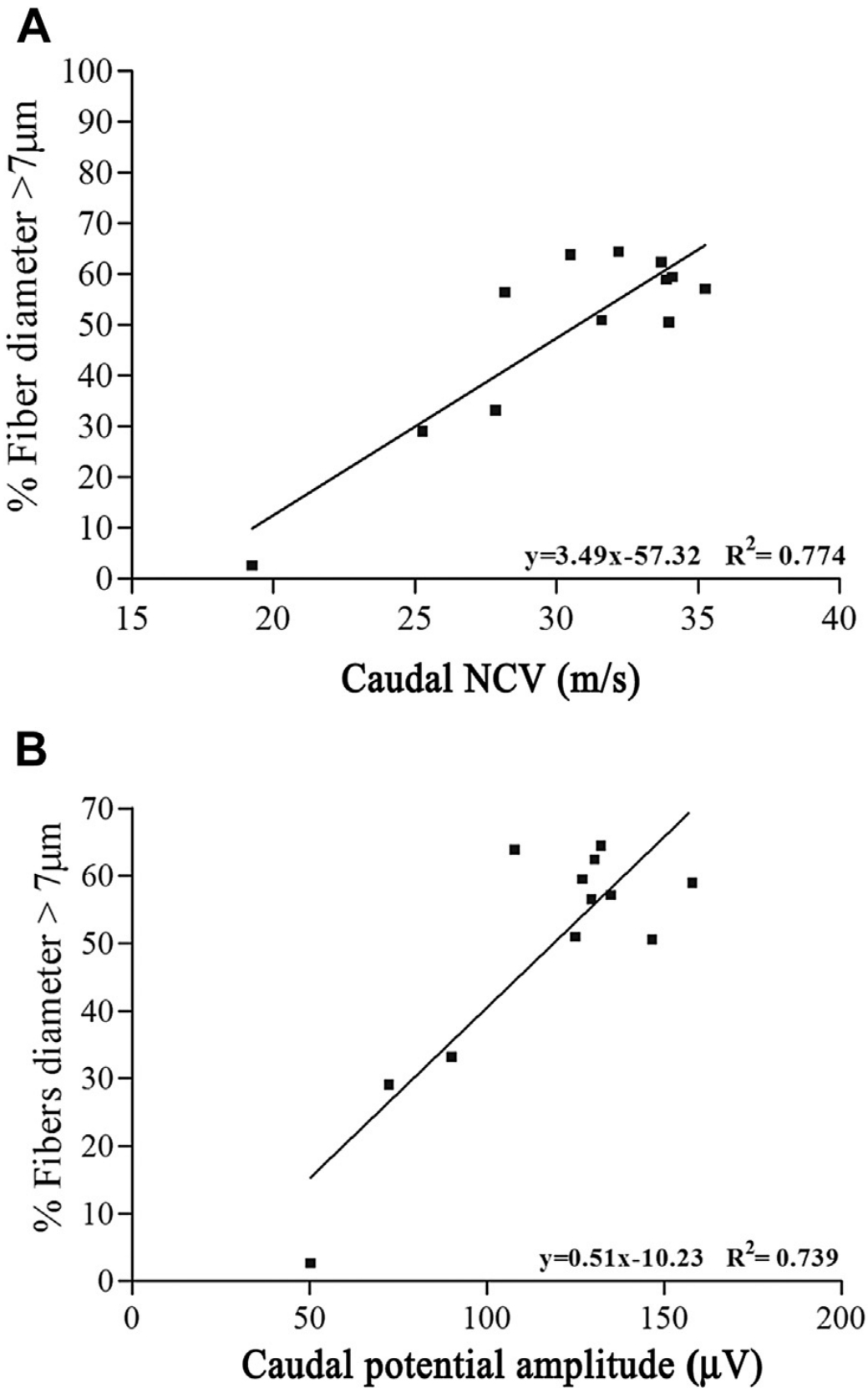

Supplementary Figure 2: Linear correlation between myelinated fibers size and conduction velocity (NCV, A) and potential amplitude (B) in the caudal nerve.

References

Beghi, E., Monticelli, M.L. 1998. Chronic symmetric symptomatic polyneuropathy in the elderly: a field screening investigation of risk factors for polyneuropathy in two Italian communities. Italian General Practitioner Study Group (IGPST). J Clin Epidemiol 51(8), 697-702.

Bharucha, N.E., Bharucha, A.E., Bharucha, E.P. 1991. Prevalence of peripheral neuropathy in the Parsi community of Bombay. Neurology 41(8), 1315-7.

Bianchi, R., Buyukakilli, B., Brines, M., Savino, C., Cavaletti, G., Oggioni, N., Lauria, G., Borgna, M., Lombardi, R., Cimen, B., Comelekoglu, U., Kanik, A., Tataroglu, C., Cerami, A., Ghezzi, P. 2004. Erythropoietin both protects from and reverses experimental diabetic neuropathy. Proc Natl Acad Sci U S A 101(3), 823-8.

Bouche, P., Cattelin, F., Saint-Jean, O., Leger, J.M., Queslati, S., Guez, D., Moulonguet, A., Brault, Y., Aquino, J.P., Simunek, P. 1993. Clinical and electrophysiological study of the peripheral nervous system in the elderly. J Neurol 240(5), 263-8.

Canta, A., Chiorazzi, A., Carozzi, V., Meregalli, C., Oggioni, N., Sala, B., Crippa, L., Avezza, F., Forestieri, D., Rotella, G., Zucchetti, M., Cavaletti, G. 2011. In vivo comparative study of the cytotoxicity of a liposomal formulation of cisplatin (lipoplatin™). Cancer Chemother Pharmacol 68(4), 1001-8. doi:10.1007/s00280-011-1574-3.

Carozzi, V.A., Canta, A., Oggioni, N., Sala, B., Chiorazzi, A., Meregalli, C., Bossi, M., Marmiroli, P., Cavaletti, G. 2010. Neurophysiological and neuropathological characterization of new murine models of chemotherapy-induced chronic peripheral neuropathies. Experimental Neurology 226(2), 301-9. doi:10.1016/j.expneurol.2010.09.004.

Carozzi, V.A., Chiorazzi, A., Canta, A., Meregalli, C., Oggioni, N., Cavaletti, G., Marmiroli, P. 2015. Chemotherapy-induced peripheral neurotoxicity in immune-deficient mice: new useful ready-to-use animal models. Exp Neurol 264, 92-102. doi:10.1016/j.expneurol.2014.11.002.

Cavaletti, G., Carozzi, V., Chiorazzi, A., Oggioni, N., Rodriguez-Menendez, V., Avezza, F., Marmiroli, P. 2013. Chemotherapy-induced peripheral neuropathy in immunodeficient mice: New useful ready-to-use animal models. Italian Journal of Anatomy and Embryology 118(2 SUPPL).

Cavaletti, G., Tredici, G., Marmiroli, P., Petruccioli, M.G., Barajon, I., Fabbrica, D. 1992. Morphometric study of the sensory neuron and peripheral nerve changes induced by chronic cisplatin (DDP) administration in rats. Acta Neuropathologica 84(4), 364-71. doi:10.1007/BF00227662.

Ceballos, D., Cuadras, J., Verdú, E., Navarro, X. 1999. Morphometric and ultrastructural changes with ageing in mouse peripheral nerve. J Anat 195 (Pt 4), 563-76.

Chentanez, V., Agthong, S., Huanmanop, T., Pairoh, S., Kaewsema, A. 2010. Morphometric analysis of the human superficial radial nerve. Anat Sci Int 85(3), 167-70. doi:10.1007/s12565-010-0073-7.

de Vito, G., Bifone, A., Piazza, V. 2012. Rotating-polarization CARS microscopy: combining chemical and molecular orientation sensitivity. Opt Express 20(28), 29369-77.

de Vito, G., Canta, A., Marmiroli, P., Piazza, V. 2015. A large-field polarisation-resolved laser scanning microscope: applications to CARS imaging. J Microsc. doi:10.1111/jmi.12282.

de Vito, G., Tonazzini, I., Cecchini, M., Piazza, V. 2014. RP-CARS: label-free optical readout of the myelin intrinsic healthiness. Opt Express 22(11), 13733-43.

Deshpande, N., Metter, E.J., Ling, S., Conwit, R., Ferrucci, L. 2008. Physiological correlates of age-related decline in vibrotactile sensitivity. Neurobiol Aging 29(5), 765-73. doi:10.1016/j.neurobiolaging.2006.12.002.

Dutta, S., Sengupta, P. 2015. Men and mice: Relating their ages. Life Sci. doi:10.1016/j.lfs.2015.10.025.

Fahrenkamp, I., Friede, R.L. 1987. Characteristic variations of relative myelin sheath thickness in 11 nerves of the rat. Anat Embryol (Berl) 177(2), 115-21.

Fujimaki, Y., Kuwabara, S., Sato, Y., Isose, S., Shibuya, K., Sekiguchi, Y., Nasu, S., Noto, Y., Taniguchi, J., Misawa, S. 2009. The effects of age, gender, and body mass index on amplitude of sensory nerve action potentials: multivariate analyses. Clin Neurophysiol 120(9), 1683-6. doi:10.1016/j.clinph.2009.06.025.

Gregg, E.W., Sorlie, P., Paulose-Ram, R., Gu, Q., Eberhardt, M.S., Wolz, M., Burt, V., Curtin, L., Engelgau, M., Geiss, L., survey, -.n.h.a.n.e. 2004. Prevalence of lower-extremity disease in the US adult population >=40 years of age with and without diabetes: 1999-2000 national health and nutrition examination survey. Diabetes Care 27(7), 1591-7.

Jacobs, J.M., Love, S. 1985. Qualitative and quantitative morphology of human sural nerve at different ages. Brain 108 (Pt 4), 897-924.

Jeronimo, A., Jeronimo, C.A., Rodrigues Filho, O.A., Sanada, L.S., Fazan, V.P. 2008. A morphometric study on the longitudinal and lateral symmetry of the sural nerve in mature and aging female rats. Brain Res 1222, 51-60. doi:10.1016/j.brainres.2008.05.055.

Knox, C.A., Kokmen, E., Dyck, P.J. 1989. Morphometric alteration of rat myelinated fibers with aging. J Neuropathol Exp Neurol 48(2), 119-39.

Komiyama, A., Suzuki, K. 1992. Age-related differences in proliferative responses of Schwann cells during Wallerian degeneration. Brain Res 573(2), 267-75.

Krinke, G.J., Herrmann, A., Körner, A., Landes, C., Sauner, F. 2014. Experience with examination of the spinal cord and peripheral nervous system (PNS) in mice: A brief overview. Exp Toxicol Pathol 66(7), 277-80. doi:10.1016/j.etp.2014.04.005.

Lauria, G., Bakkers, M., Schmitz, C., Lombardi, R., Penza, P., Devigili, G., Smith, A.G., Hsieh, S.T., Mellgren, S.I., Umapathi, T., Ziegler, D., Faber, C.G., Merkies, I.S. 2010. Intraepidermal nerve fiber density at the distal leg: a worldwide normative reference study. J Peripher Nerv Syst 15(3), 202-7. doi:10.1111/j.1529-8027.2010.00271.x.

Lauria, G., Lombardi, R., Borgna, M., Penza, P., Bianchi, R., Savino, C., Canta, A., Nicolini, G., Marmiroli, P., Cavaletti, G. 2005. Intraepidermal nerve fiber density in rat foot pad: neuropathologic-neurophysiologic correlation. J Peripher Nerv Syst 10(2), 202-8. doi:10.1111/j.1085-9489.2005.0010210.x.

Leblhuber, F., Schroecksnadel, K., Beran-Praher, M., Haller, H., Steiner, K., Fuchs, D. 2011. Polyneuropathy and dementia in old age: common inflammatory and vascular parameters. J Neural Transm (Vienna) 118(5), 721-5. doi:10.1007/s00702-011-0579-8.

Manini, T.M., Clark, B.C. 2012. Dynapenia and aging: an update. J Gerontol A Biol Sci Med Sci 67(1), 28-40. doi:10.1093/gerona/glr010.

Mardia, K. V., Jupp, P.E. Directional Statistics. Hoboken: Wiley; 1999.

Martyn, C.N., Hughes, R.A. 1997. Epidemiology of peripheral neuropathy. J Neurol Neurosurg Psychiatry 62(4), 310-8.

Melcangi, R.C., Azcoitia, I., Ballabio, M., Cavarretta, I., Gonzalez, L.C., Leonelli, E., Magnaghi, V., Veiga, S., Garcia-Segura, L.M. 2003. Neuroactive steroids influence peripheral myelination: a promising opportunity for preventing or treating age-dependent dysfunctions of peripheral nerves. Prog Neurobiol 71(1), 57-66.

Melcangi, R.C., Magnaghi, V., Cavarretta, I., Martini, L., Piva, F. 1998. Age-induced decrease of glycoprotein Po and myelin basic protein gene expression in the rat sciatic nerve. Repair by steroid derivatives. Neuroscience 85(2), 569-78.

Meregalli, C., Carozzi, V.A., Sala, B., Chiorazzi, A., Canta, A., Oggioni, N., Rodriguez-Menendez, V., Ballarini, E., Ceresa, C., Nicolini, G., Crippa, L., Orciani, M., Cavaletti, G., Marmiroli, P. 2015. Bortezomib-induced peripheral neurotoxicity in human multiple myeloma-bearing mice. J Biol Regul Homeost Agents 29(1), 115-24.

Mold, J.W., Vesely, S.K., Keyl, B.A., Schenk, J.B., Roberts, M. 2004. The prevalence, predictors, and consequences of peripheral sensory neuropathy in older patients. J Am Board Fam Pract 17(5), 309-18.

Monticelli, M.L., Beghi, E. 1993. Chronic symmetric polyneuropathy in the elderly. A field screening investigation in two regions of Italy: background and methods of assessment. The Italian General Practitioner Study Group (IGPSG). Neuroepidemiology 12(2), 96-105.

Renn, C.L., Carozzi, V.A., Rhee, P., Gallop, D., Dorsey, S.G., Cavaletti, G. 2011. Multimodal assessment of painful peripheral neuropathy induced by chronic oxaliplatin-based chemotherapy in mice. Mol Pain 7, 29. doi:10.1186/1744-8069-7-29.

Richardson, J.K. 2002. The clinical identification of peripheral neuropathy among older persons. Arch Phys Med Rehabil 83(11), 1553-8.

Savettieri, G., Rocca, W.A., Salemi, G., Meneghini, F., Grigoletto, F., Morgante, L., Reggio, A., Costa, V., Coraci, M.A., Di Perri, R. 1993. Prevalence of diabetic neuropathy with somatic symptoms: a door-to-door survey in two Sicilian municipalities. Sicilian Neuro-Epidemiologic Study (SNES) Group. Neurology 43(6), 1115-20.

Schmelzer, J.D., Low, P.A. 1987. Electrophysiological studies on the effect of age on caudal nerve of the rat. Exp Neurol 96(3), 612-20.

Schmidt, R.E., Dorsey, D., Parvin, C.A., Beaudet, L.N., Plurad, S.B., Roth, K.A. 1997. Dystrophic axonal swellings develop as a function of age and diabetes in human dorsal root ganglia. J Neuropathol Exp Neurol 56(9), 1028-43.

Serra, J. Image Analysis and Mathematical Morphology. London: Academic Press; 1982

Shen, D., Zhang, Q., Gao, X., Gu, X., Ding, F. 2011. Age-related changes in myelin morphology, electrophysiological property and myelin-associated protein expression of mouse sciatic nerves. Neurosci Lett 502(3), 162-7. doi:10.1016/j.neulet.2011.07.034.

Soltanpour, N., Asghari Vostacolaee, Y., Pourghasem, M. 2012. Comparison of Morphometric Aspects of Light and Electron Microscopy of the Hypoglossal Nerve between Young and Aged Male Wistar Rats. Cell J 13(4), 229-36.

Suzuki, M. 2013. Peripheral neuropathy in the elderly. Handb Clin Neurol 115, 803-13. doi:10.1016/B978-0-444-52902-2.00046-1.

Tanaka, K., Zhang, Q.L., Webster, H.D. 1992. Myelinated fiber regeneration after sciatic nerve crush: morphometric observations in young adult and aging mice and the effects of macrophage suppression and conditioning lesions. Exp Neurol 118(1), 53-61.

van Nes, S.I., Faber, C.G., Hamers, R.M., Harschnitz, O., Bakkers, M., Hermans, M.C., Meijer, R.J., van Doorn, P.A., Merkies, I.S., Group, P.S. 2008. Revising two-point discrimination assessment in normal aging and in patients with polyneuropathies. J Neurol Neurosurg Psychiatry 79(7), 832-4. doi:10.1136/jnnp.2007.139220.

Verdú, E., Butí, M., Navarro, X. 1996. Functional changes of the peripheral nervous system with aging in the mouse. Neurobiol Aging 17(1), 73-7.

Verdú, E., Ceballos, D., Vilches, J.J., Navarro, X. 2000. Influence of aging on peripheral nerve function and regeneration. J Peripher Nerv Syst 5(4), 191-208.

Ward, R.E., Boudreau, R.M., Caserotti, P., Harris, T.B., Zivkovic, S., Goodpaster, B.H., Satterfield, S., Kritchevsky, S., Schwartz, A.V., Vinik, A.I., Cauley, J.A., Newman, A.B., Strotmeyer, E.S., study, H.A. 2015. Sensory and motor peripheral nerve function and longitudinal changes in quadriceps strength. J Gerontol A Biol Sci Med Sci 70(4), 464-70. doi:10.1093/gerona/glu183.

Ward, R.E., Boudreau, R.M., Caserotti, P., Harris, T.B., Zivkovic, S., Goodpaster, B.H., Satterfield, S., Kritchevsky, S.B., Schwartz, A.V., Vinik, A.I., Cauley, J.A., Simonsick, E.M., Newman, A.B., Strotmeyer, E.S., Health, A.i.a.B.C.S. 2014. Sensory and motor peripheral nerve function and incident mobility disability. J Am Geriatr Soc 62(12), 2273-9. doi:10.1111/jgs.13152.